Journal of The Electrochemical Society, **156** (7) E118-E123 (2009)
0013-4651/2009/156(7)/E118/6/$25.00 © The Electrochemical Society

Electrochemical Analysis of H_2O_2 and Nitrite Using Copper Nanoparticles/Poly(*o*-phenylenediamine) Film Modified Glassy Carbon Electrode

S. Ashok Kumar, Po-Hsun Lo, and Shen-Ming Chen[*,z]

Department of Chemical Engineering and Biotechnology, National Taipei University of Technology, Taipei 106, Taiwan

Copper nanoparticles (Cu-NPs) have been electrochemically synthesized onto a poly(*o*-phenylenediamine) (PoPD-) coated glassy carbon electrode (GCE). Electrochemical properties and surface characterizations were studied using cyclic voltammetry, atomic force microscopy (AFM), scanning electron microscopy (SEM), and X-ray diffraction (XRD) analysis. Cyclic voltammetry, AFM, SEM, and XRD confirmed the presence of Cu-NPs on the electrode surface. Cu-NPs are firmly stabilized by surface attachment of the PoPD functionality that can be attached to the electrode surface, thus becoming an integral part of the polymer backbone. The Cu-NPs–polymer film-coated GCE (Cu-NPs/PoPD/GCE) showed excellent electrocatalytic activity toward the reduction of hydrogen peroxide (H_2O_2) and nitrite (NO_2^-). Amperometry was carried out to determine the concentration of H_2O_2 and NO_2^- at −0.3 V. The dependence of the current response on the H_2O_2 concentration was explored under neutral conditions, and an excellent linear concentration range from 1.0×10^{-6} to 1.0×10^{-3} M was found. The Cu-NPs/PoPD/GCE allows highly sensitive, low working potential, stable, and fast amperometric sensing of H_2O_2 and NO_2^-. This is promising for the future development of nonenzymatic sensors. The real-sample analysis of commercial H_2O_2 samples was performed using the proposed method, and the obtained results are satisfactory.
 [DOI: 10.1149/1.3129604]

Manuscript submitted October 21, 2008; revised manuscript received January 18, 2009. Published May 21, 2009.

Electrodes modified with nanoscale materials are widely used for the fabrication of chemical and biosensors. Because our aim is to prepare a reliable, reproducible, selective, and fast monitoring sensor for a specific analyte, for this purpose, nanoparticles (NPs) are promising tools because they could facilitate electron-transfer reactions, and this could be coupled with ease of miniaturization of sensing devices to nanoscale dimensions. Nanoparticles are suitable for important applications in chemical/biochemical sensing because of their high surface-to-volume ratio and highly effective catalytic properties.[1-10]

The development of a hydrogen peroxide (H_2O_2) sensor has been considered important in biomedical and environmental applications. It is necessary to determine H_2O_2 not only in chemical and industrial processes such as disinfection and wastewater treatment, but also as an intermediate product of an enzyme reaction in biochemical processes.[11,12] For this purpose, many types of H_2O_2 sensors have been developed. In practice, measuring H_2O_2 by using electrochemical sensors is more advisable because of its simplicity, low cost, and suitability for field analysis.[13,14] Recently, enzyme-based sensors[15-19] and nonenzymatic[20-24] electrochemical sensors were reported for the detection of H_2O_2.

Nitrite ions are produced as an intermediate during the biodegradation of nitrogenous wastes and in effluents from various industries. Nitrite is ubiquitous within environmental, food, industrial, and physiological systems. Electrochemical reduction of nitrite and its determination are of environmental importance. The products of the electrochemical reduction of nitrites depend on the conditions of the reduction such as electrode material, pH, coexisting ions, etc.[25-27] A review deals with the analytical methods reported for nitrite determination.[28] Recently, a sensitive and selective kinetic method was developed for the determination of nitrite,[29] a nitrite determination was based on a horseradish peroxidase/catalase biosensor,[30] and a sandwich-structured SiO_2/cytochrome c/SiO_2 on a boron-doped diamond film electrode[31] was reported.

In recent years there have been many studies on the incorporation of metal particles within a conducting polymer matrix, such as polyaniline or polypyrrole.[32-37] This incorporation can be achieved readily by the reduction of the appropriate metal salt at the conducting polymer interface. The interest in these materials lies in the fact that they are promising materials in the fields of catalysis and electrocatalysis. By this strategy, the incorporation of noble metals within the porous polymer matrix produces a highly dispersed noble-metal catalyst with a greater surface area and a much lower probability of agglomeration of the metal particles.[38-40]

In the present work, we have prepared copper NPs on a poly(*o*-phenylenediamine) (PoPD) film-coated electrode. Surface characterizations were performed using X-ray diffraction (XRD), scanning electron microscopy (SEM), and atomic force microscopy (AFM). Electrochemical and electrocatalytic properties of Cu-NPs/PoPD nanocomposite modified electrodes were tested. The Cu-NPs/PoPD/glassy carbon electrode (GCE) shows an excellent electrocatalytic activity toward H_2O_2 and nitrite. Using amperometry, the linear range and detection limit for H_2O_2 and nitrite were estimated.

Experimental

Reagents and apparatus.— *o*-Phenylenediamine was purchased from Sigma-Aldrich (St. Louis, MO). Hydrogen peroxide (30%, w/w), sodium nitrite, sodium hydroxide, sodium sulfate, potassium ferrocyanide, potassium ferricyanide, lithium perchlorate, and sodium hydroxide were purchased from Wako Pure Chemicals (Osaka, Japan). Sodium acetate and sodium dihydrogen phosphate were received from E-Merck (Darmstadt, Germany). Copper sulfate pentahydrate was received from Ishizu Seiyaku Ltd. (Osaka, Japan), and other chemicals were of analytical grade and used without further purification. Double-distilled water was used in all experiments. Diluted H_2O_2 standard solutions were freshly prepared directly before use.

Electrochemical measurements were performed by a CHI750A Electrochemical Work Station. GCEs from BAS and indium tin oxide-coated glass electrodes were purchased from Merck Display Technologies Ltd. Platinum wire was used as the counter electrode. All cell potentials were measured with respect to a Ag/AgCl [KCl (sat.)] reference electrode. AFM images were recorded with a multimode scanning probe microscope system operated in tapping mode using Beijing Nano-Instruments CSPM-4000 (Ben Yuan Ltd., Beijing, China). X'Pert PRO Diffractometer (PANalytical, Almelo) with Cu radiation was used for XRD analysis. A Hitachi Scientific Instruments (London, U.K.) model S-3000H scanning electron microscope was used for surface image measurements. Electrochemical impedance measurements were performed using an impedance measurement unit, IM6ex ZAHNER, Messsysteme (Kroanch, Germany). All pH measurements were performed with a Suntex model

* Electrochemical Society Active Member.
z E-mail: smchen78@ms15.hinet.net

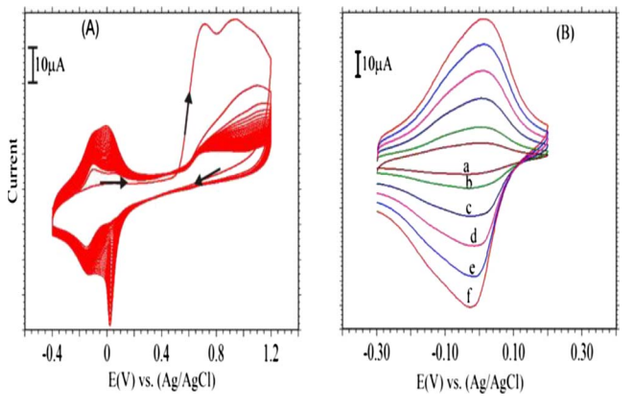

Figure 1. (Color online) (A) CVs for deposition of PoPD film onto GCE from an electrolyte containing 2.5×10^{-2} M *o*-phenylenediamine and 0.1 M Na_2SO_4 (pH 1), scan rate = 50 mV/s. (B) CVs of PoPD/GCE in an aqueous electrolyte containing H_2SO_4 + Na_2SO_4 (pH 1). Scan rate: (a) 10, (b) 20, (c) 40, (d) 60, (e) 80, and (f) 100 mV/s.

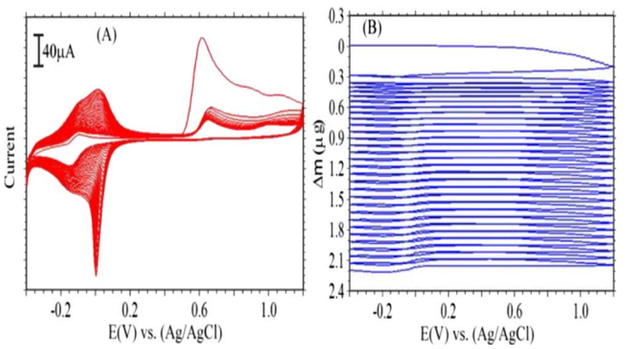

Figure 2. (Color online) (A) CVs of PoPD film formation onto a Au-coated quartz crystal electrode from a pH 1.0 aqueous, 0.1 M Na_2SO_4 solution containing 2.5×10^{-2} M *o*-phenylenediamine. (B) The mass changes on a Au quartz crystal in EQCM measurements. Scan rate = 0.02 V/s.

SP-701 pH meter (Jiangsu, China). The working electrode for the electrochemical quartz crystal microbalance (EQCM) measurement was an unpolished AT-cut Au-coated 8 MHz quartz crystal (purchased from CH Instruments). The diameter of the quartz crystal was 13.7 mm and the gold electrode diameter was 5 mm. Before use, the Au-coated quartz crystal surfaces were cleaned by exposure to piranha solution (one part of 30% H_2O_2 in three parts of H_2SO_4) for 2 min, rinsed with pure water, and then dried in a nitrogen environment. All experiments were carried out at an ambient temperature of 25 ± 2°C.

Electrode modification.— The GCE working electrode was polished carefully with alumina powder (0.05 μm) on a soft polishing cloth (Buehler). After sonicating in absolute ethanol, then in water for 5 min, successively, it was treated with cyclic scanning in the potential range from −0.5 to 1.2 V at the scan rate of 0.1 V s^{-1} in 0.1 M H_2SO_4 until a stable cyclic voltammogram for a clean GCE was obtained. The electrodeposition of PoPD was carried out from a nitrogen-purged aqueous electrolyte solution containing 2.5×10^{-2} M *o*-phenylenediamine monomer and 0.1 M Na_2SO_4 (pH 1) by cycling the potential between −0.40 and +1.20 V at 0.05 V s^{-1}. A thin film made with 30 deposition cycles was used in all experiments. When removed from the solution, the PoPD modified GCE was rinsed with distilled water to remove unbound materials from the electrode surface and then dried by nitrogen gas.

Cu-NPs deposition.— Cu-NPs were deposited electrochemically onto PoPD-coated GCEs from solutions of 0.01 M $CuSO_4$ + 0.1 M $NaClO_4$ under different applied potentials from −0.4 to −1.4 V (vs Ag/AgCl).[40] After the modification with Cu-NPs, the electrode was thoroughly washed to remove unbound materials from the electrode surface and then was dried in air for 30 min.

Results and Discussion

Electrochemical deposition of PoPD.— The consecutive cyclic voltammograms (CVs) recorded by using GCEs dipped in a mixture containing 2.5×10^{-2} M *o*-phenylenediamine and 0.1 M Na_2SO_4 (pH adjusted to 1 using H_2SO_4) under nitrogen-saturated conditions showed an oxidation peak at 0.7 V (Fig. 1A). In the subsequent cycles, the oxidation current decreased at 0.7 V with a simultaneous appearance of a redox wave at ($E^{0'}$) 0.02 V due to the formation of PoPD. This clearly shows the oxidation of the *o*-phenylenediamine and the formation of a PoPD film on the GCE. This result is in good agreement with previous reports.[41-43] According to the proposed mechanism for the electropolymerization of *o*-phenylenediamine, the monomer was initially oxidized anodically to give the monocation radical, which then underwent chemical coupling to produce a dimer that could be further oxidized. The dication of the dimer could undergo either polymerization to produce a linear chain polymer or become cyclized to yield a ladder structure of a phenazine ring through the polymerization of the oxidized products.[41,44-46]

Figure 1B shows the CVs of the PoPD/GCE electrode in a N_2-saturated aqueous electrolyte containing 0.1 M H_2SO_4 and 0.1 M Na_2SO_4 (pH 1) at different scan rates. It is clear that the peak current increases as the scan rate, ν, increases, while the peak potential is practically insensitive to the change in ν, and the peak separation (ΔE_p) is nearly 0.04 V. Within the tested ν range (10–100 mV/s), the peak current, i_p, varies linearly with ν as can be seen in Fig. 1B. This indicates that the electroactivity of the PoPD film in 0.1 M H_2SO_4 + 0.1 M Na_2SO_4 (pH 1) is similar to that of surface-attached electroactive sites.[47]

The EQCM is a powerful instrument that is capable of detecting very small mass changes on the Au-coated quartz crystal electrode's surface that accompanies the electrochemical process occurring on the electrode surface. EQCM is an extremely sensitive sensor capable of measuring the mass changes in the nanogram range on the quartz crystal. Typical EQCM experiments were performed and changes in mass were recorded concurrently with the consecutive CVs over scanning cycles between 0.4 and 1.2 V in H_2SO_4 + Na_2SO_4 (pH 1) containing 2.5×10^{-2} M *o*-phenylenediamine at a scan rate of 0.02 V s^{-1} (Fig. 2A and B). Sauerbrey's equation (Eq. 1) was used to calculate mass loadings on the quartz crystal[48,49]

$$\text{change in mass } (\Delta f) = -(2f_0^2/A\sqrt{\mu\rho})\Delta m \qquad [1]$$

where A is the piezoelectricity area (0.196 cm^2), ρ is the quartz density (2.648 g cm^{-3}), μ is the shear modulus (2.947×10^{11} dyne cm^{-2} for AT-cut quartz), and f_0 is the resonance frequency of the quartz crystal can be used to calculate the changes of the mass (Δm) taking place at the electrode surface from the changes of the resonance frequency (Δf) of the quartz crystal.

Figure 2B shows that the corresponding mass changes for the EQCM recorded during the electrochemical deposition of PoPD using the consecutive cyclic voltammetry. The increases in the mass noticed in Fig. 2B are consistent with the growth of the PoPD film on the gold electrode. This experimental result confirmed that the deposition potential for PoPD film formation mainly occurred between +0.6 and +1.2 V (vs Ag/AgCl), and the total mass of PoPD was found to be 2.153 μg. Figure 3A and B demonstrates the CVs and the corresponding mass changes during Cu-NPs deposition onto PoPD-coated Au from solutions of 0.01 M $CuSO_4$ + 0.1 M $NaClO_4$ under different applied potentials from −0.4 to −1.4 V (vs Ag/AgCl). As observed in Fig. 3B, the major mass changes were observed from −0.40 to −1.2 V, which confirmed that Cu-NP deposition occurred.[40] However, the cathodic current increased up to −1.7

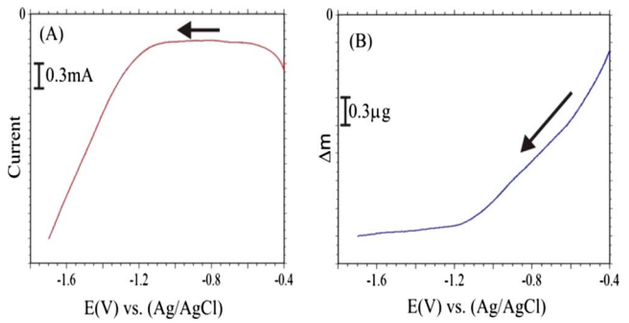

Figure 3. (Color online) (A) CVs of Cu-NPs deposition onto PoPD/Au-coated quartz crystal electrode from an aqueous solution containing 0.01 M $CuSO_4$ + 0.1 M $NaClO_4$. (B) The mass changes during Cu-NPs deposition onto PoPD/Au quartz crystal in EQCM measurements. Scan rate = 0.02 V/s.

V because of the hydrogen evolution reaction at higher cathodic peak potential.[50,51] This observation was supported by earlier reports,[50,51] and they found that a continuous mass increase is observed as the potential is scanned in the cathodic direction during the deposition of Cu-NPs. After the frequency change during the potential scanning from −0.4 to −1.7 V, the amount of Cu NPs deposited on the PoPD film was estimated to be +422 ng.

The loading mass of Cu-NPs on a PoPD modified electrode was evaluated by varying the deposition cycles. The CVs were recorded in a 0.1 M phosphate buffer solution (PBS) after the deposition of Cu-NPs on a PoPD modified electrode by changing the scanning cycles. It can be observed that the response current of the Cu-NPs/PoPD/GCE first increased with the increase of Cu-NP loading. However, the size of the copper particles also increased with the increase of sweeping cycles, and larger sized particles decrease the catalytic activity of copper particles. As we observed from SEM (Fig. 4b) and AFM (Fig. 4c and d) studies, the highly uniform Cu-NPs were observed for single sweeping deposition. Based on these observations, we selected a single sweeping (from −0.4 to −1.7) for the deposition of Cu-NPs on a PoPD modified electrode throughout this study.

Surface characterizations.— As shown in Fig. 4a, Cu(111) and (200) peaks were observed in XRD results of Cu-NPs. The peaks of the XRD pattern for the sample in Fig. 4a can be readily indexed to a cubic phase of Cu-NPs; the reflection peaks at 2θ = 43.44 and 50.64 are indexed as [111] and [200] planes of copper, respectively, in good agreement with the reported data.[52] Using SEM, the Cu-NPs/PoPD film modified electrode was investigated and, from the SEM image shown in Fig. 4b, Cu-NPs and PoPD films were confirmed on the electrode surface. Figure 4c and d shows the AFM images of Cu-NPs deposited on a polymer-modified electrode. The AFM topography image clearly predicted the homogeneous dispersion of Cu-NPs, and the particle sizes were found to be in the range of 100 ± 25 nm. The phase diagram shows the Cu-NPs (Fig. 4d) embedded into the polymer film uniformly. Using an AFM image analyzer, the approximate film thickness was found to be 80 nm.

Electrochemical studies.— Electrochemical impedance spectroscopy (EIS) was used to further characterize the modified electrodes. The modification of the electrode surfaces by a resistive monolayer results in their passivation and, hence, alters their ac response. In terms of a Randles equivalent circuit, two components are affected: At high frequencies, where the electrode reaction is purely kinetic controlled, the heterogeneous charge-transfer resistance is expected to increase due to the inhibition of the electron-transfer rate; at lower frequencies, the Warburg impedance is expected to deviate from a linear dependence on $\omega^{-1/2}$. Figure 5 shows the impedance spectra of Cu-NPs/PoPD/GCEs, PoPD/GCEs, and bare GCEs in 5 mM $[Fe(CN)_6]^{3-/4-}$ in 0.1 M KCl solution. It can be seen that the bare GCE electrode shows a low frequency straight line with a very small semicircle (diameter = 103 Ω) at high frequencies, indicating a diffusion-controlled process for the redox couple (Fig. 5, curve c). The Nyquist plots recorded in the presence of the only PoPD–polymer film-coated GCE show a very small semicircle in the high frequency region (curve b). However, the Cu-NPs/PoPD/GCE

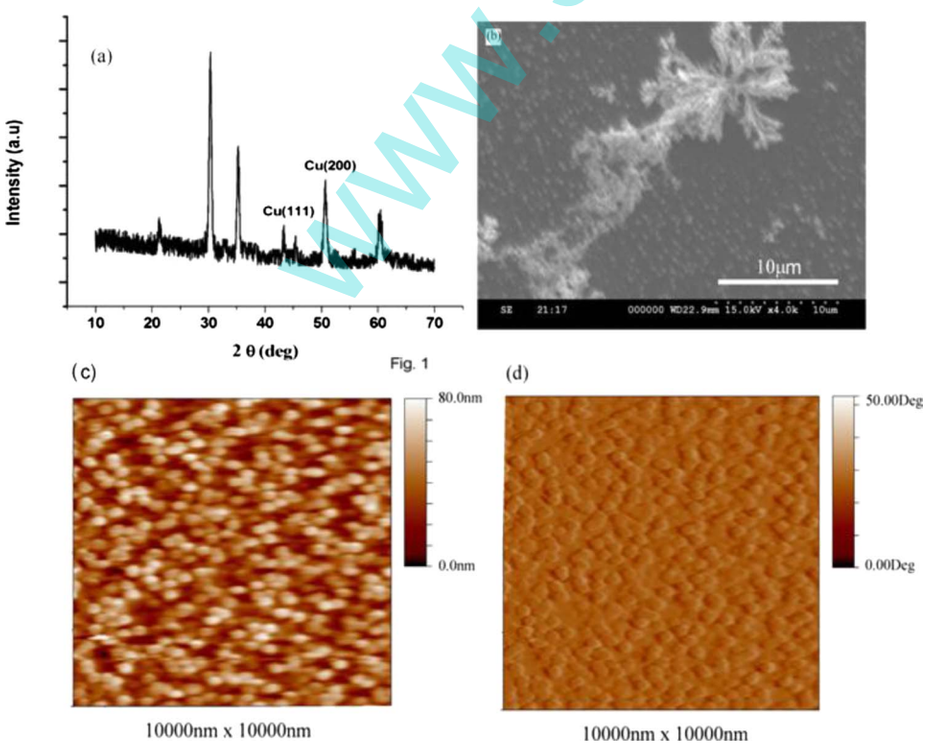

Figure 4. (Color online) (a) XRD images of Cu-NPs on a PoPD film. (b) SEM image of a Cu-NPs/PoPD film-coated electrode. (c) AFM images of a Cu-NPs/PoPD film-coated electrode. (d) Topography image.

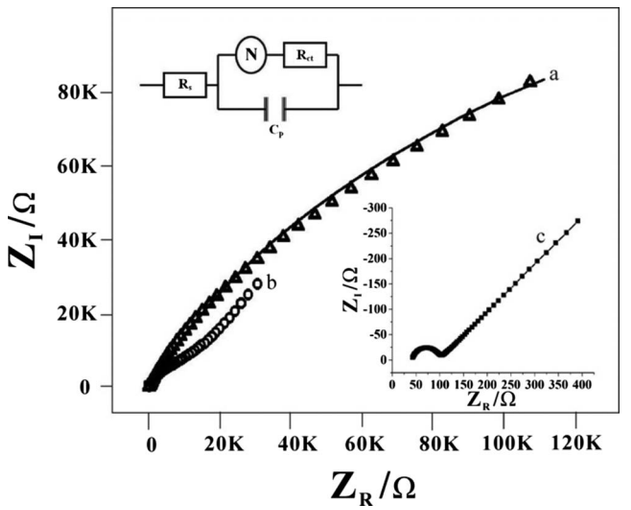

Figure 5. EIS of Cu-NPs/PoPD/GCE (curve a), PoPD/GCE (curve b), and bare GCE (curve c) in 5 mM $[Fe(CN)_6]^{3-/4-}$ + 0.1 M KCl solution.

showed a straight line from higher frequency to lower frequency (curve a). The presence of the straight line from lower to higher frequencies agrees with the lack of complete blocking under the experimental conditions of this work. The decreasing charge-transfer resistance for the Cu-NPs/PoPD/GCE is because Cu-NPs can act as an electron-transfer medium with an enhanced electron-transfer rate also indicates that Cu-NPs had been attached to the PoPD/GCE surface. The impedance spectra were fitted to a standard Randle equivalent circuit consisting of a parallel combination of a capacitor (C) and Nernst impedance (N) in series with the charge-transfer resistance, R_{ct}. The solution resistance (R_s) is a series combination of charge-transfer resistance R_{ct} and the Nernst impedance (N). This circuit models a cell where polarization is due to a combination of kinetic and diffusion processes (inset of Fig. 5). The Nyquist plot for this circuit is shown in Fig. 5, curve a. The following values were obtained: (N) = 64.66 Warburg impedance of constant diffusion, C = 279.2 nF, R_s = 70.4 Ω, and R_{ct} = 232.6 kΩ. These results indicate that electron transfer is highly promoted in the presence of Cu-NPs on the electrode surface.

Figure 6A shows the CVs recorded in 0.1 M PBS, (pH 7.0) using a PoPD/GCE (curve a), Cu-NPs/PoPD/GCE (curve b), and a bare Cu electrode (curve c). The Cu-NPs/PoPD/GCE shows (curve b) two cathodic peaks (C1 at −0.11 V and C2 at −0.15 V) and an

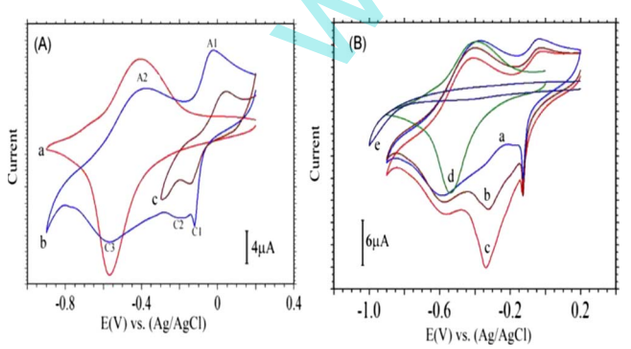

Figure 6. (Color online) (A) CVs of [curve (a)] PoPD/GCE, [curve (b)] Cu-NPs/PoPD/GCE, and a [curve (c)] bare Cu electrode in 0.1 M PBS. (B) CVs of Cu-NPs/PoPD/GCE modified electrodes in the (a) absence and presence of (b) 400 and (c) 600 μM H_2O_2. A PoPD/GCE in the presence of 600 μM H_2O_2 (curve d). Scan rate: 20 mV s^{-1}; supporting electrolyte: 0.1 M PBS (pH 7.0).

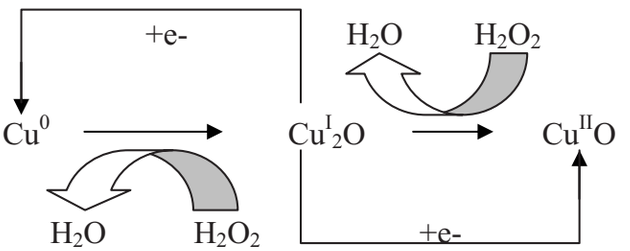

Scheme 1.

anodic peak (A1 at −0.03 V). Only a single peak corresponding to the total redox transition of CuO/Cu could be obtained when the scan rate was higher than 40 mV. According to the reports, C1 and C2 correspond to $Cu^{II}O \rightarrow Cu^I_2O$ and $Cu^I_2O \rightarrow Cu^0$, respectively, and the anodic peak (A1) comes from the formation of Cu_2O and CuO multilayers.[53-55] Another reduction peak C3 (−0.54 V) and oxidation peak A2 (−0.34 V) correspond to the redox reaction of PoPD.[56] From these data, we confirmed that Cu-NPs are incorporated into the polymer film.

Electrocatalytic reduction of H_2O_2.— To investigate the electrocatalytic activity of the Cu-NPs/PoPD/GCE, electrochemical catalytic reduction of H_2O_2 was investigated by cyclic voltammetry (Fig. 6B). There was no reduction peak observed at bare GCE (curve e) and PoPD/GCE (curve d) in the presence of H_2O_2 in the potential range from 0.2 to −0.9 V, suggesting that both electrodes are inactive toward the direct reduction of H_2O_2. However, at the Cu-NPs/PoPD/GCE, the reduction peak current at about −0.30 V was greatly enhanced in the presence of H_2O_2 corresponding to the decrease in the oxidation peak current, suggesting a typical electrocatalytic reduction process of H_2O_2. The reduction peak current increased with the concentration of H_2O_2 (curves b and c). These results indicate that a mediated reduction of H_2O_2 takes place at the Cu-NPs/PoPD/GCE.[54,55] Based on the earlier reports,[54-56] the mechanism for a mediated reduction of H_2O_2 at theCu-NPs/PoPD/GCE is a coupled chemical-type reaction mechanism as shown in Scheme 1.

Amperometric determination of H_2O_2.— The Cu-NPs/PoPD/GCE was used as an amperometric detector in an electrochemical cell, and the working potential was fixed at −0.3 V. The supporting electrolyte was a 0.1 M PBS (pH 7.0). The Cu-NPs/PoPD/GCE quickly responds to dynamic changes in the H_2O_2 concentration and reaches a constant value within 3 s (Fig. 7A). With each addition of H_2O_2 the sensor gave an additional response, which clearly demonstrates that the Cu-NPs/PoPD/GCE can be employed as an amperometric detector in hydrodynamic amperometry. The relationship between the amperometric step signal and the concentration of H_2O_2 was

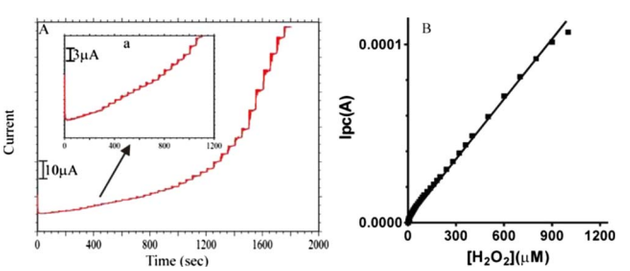

Figure 7. (Color online) (A) Amperometric responses recorded with the Cu-NPs/PoPD/GCE at −0.3 V upon successive additions of H_2O_2 in 0.1 M PBS (pH 7.0) from 1.0×10^{-6} to 1.0×10^{-3} M, rotation rate = 1000 rpm. The inset shows the magnified scale for low concentrations of H_2O_2. (B) The calibration plot of H_2O_2.

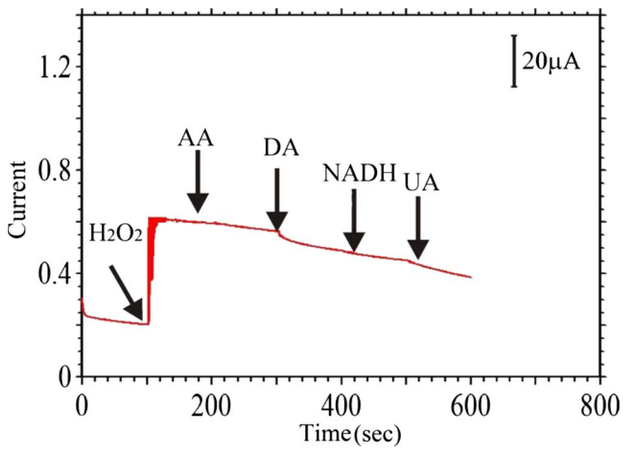

Figure 8. (Color online) Amperometric response for interferences recorded using Cu-NPs/PoPD/GCE at −0.3 V upon successive additions of 300 μM H_2O_2, 5.0 mM AA, 5.0 mM DA, 1.5 mM NADH, and 5.0 mM UA in 0.1 M PBS (pH 7.0).

investigated for the range 1.0×10^{-6} to 1.0×10^{-3} M, and a substantially low detection limit of 0.1×10^{-6} M [signal-to-noise ratio (S/N) = 3] was obtained (Fig. 7B). A linear relationship exists up to 1.0×10^{-3} M, and the linear regression equation $y(\mu A) = 0.10x + 3$ shows a correlation coefficient (r^2) of 0.999.

We measured the content of H_2O_2 in commercially available antibacterial and glass-cleaning solutions using a Cu-NPs/PoPD/GCE. The diluted H_2O_2 solution was mixed with 10 mL of PBS and then analyzed using the standard addition method. The relative standard deviation (RSD = 1.62%, n = 5) and the recovered ratio on the basis of this method were investigated and the value is between 97.33 and 99.10%. The results obtained using the proposed method (2.920%) and the manufacturer's labeled values (~3%) are in agreement.

We examined the role of common biological interferences such as ascorbic acid (AA), dopamine (DA), the reduced form of nicotinamide adenine dinucleotide (NADH), and uric acid (UA) on steady-state current measurements of H_2O_2. In this experiment the potential was kept at −0.3 V, and the amperometric response for the successive additions of 300 μM H_2O_2, 5.0 mM AA, 5.0 mM DA, 1.5 mM NADH, and 5.0 mM UA at the Cu-NPs/PoPD/GCE was recorded. It was observed that the addition of 300 μM H_2O_2 gave a fast response and the possible interferences did not show significant response at this modified electrode (Fig. 8). These results clearly indicate that AA, DA, NADH, and UA do not interfere with the steady-state current of H_2O_2 at −0.3 V.

Electrocatalytic reduction of nitrite at Cu-NPs/PoPD/GCE.— In this work, the nitrite (NO_2^-) electrocatalytic reduction at the Cu-NPs/PoPD/GCE was studied by cyclic voltammetry. Figure 9A shows CVs of the Cu-NPs/PoPD/GCE in the absence (curve a) and presence (curve b) of NO_2^-. As shown in Fig. 9A for the PoPD/GCE (curve d) and the bare GCE (curve e), no redox response of NO_2^- can be seen in the potential range from 0.3 to −0.7 V. However, at the Cu-NPs/PoPD/GCE, the reduction current was greatly increased due to catalytic reduction of NO_2^-, whereas the oxidation peak decreased. The decrease in the oxidative peak current together with the increase in the reductive peak current confirmed that the Cu-NPs on the PoPD/GCE demonstrated a catalytic ability for NO_2^- reduction. The electrochemical reduction peak current for NO_2^- was observed only under acidic conditions because at pH 1, free nitric oxide (NO) is generated in the solution containing nitrite due to the disproportionation reaction of nitrous acid[57,58]

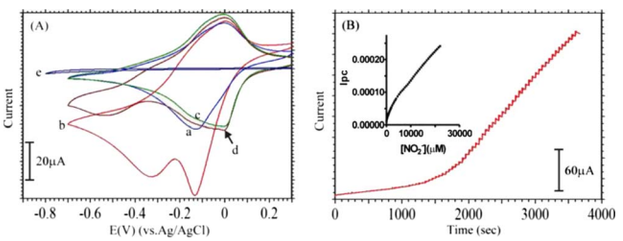

Figure 9. (Color online) (A) CVs of Cu-NPs/PoPD/GCE modified electrode in the (a) absence and (b) presence of 1.0 mM NO_2^- in 0.5 M HCl. The PoPD/GCE in [curve (c)] the absence and [curve (d)] presence of 1.0 mM NO_2^-. Scan rate: 50 mV s^{-1}. (B) Amperometric responses recorded with the Cu-NPs/PoPD/GCE at −0.3 V to the successive addition of NO_2^- in 0.5 M HCl from 5 μM to 22 mM, rotation rate = 1000 rpm. The inset shows the calibration plot of NO_2^-.

$$3HNO_2 \rightarrow H^+ + NO_3^- + 2NO + H_2O \quad [2]$$

According to earlier reports,[57,58] the proposed electrochemical reduction mechanism of generated nitric oxide at the Cu-NPs/PoPD/GCE is as follows

$$Cu(0) + NO + nH^+ \rightarrow Cu(oxidized) + NH_3 \quad [3]$$

As shown in Fig. 9B, the amperometric response of the Cu-NPs/PoPD modified glassy carbon disk electrode was recorded upon the successive addition of NO_2^- into a continuously stirred buffer solution at an applied potential of −0.3 V (vs Ag/AgCl). Upon the addition of NO_2^-, the steady-state current of the Cu-NPs/PoPD modified glassy carbon disk electrode achieved 96% of its value in less than 5 s. Such a fast response is attributed to a direct electron transfer between Cu-NPs and the PoPD glassy carbon disk electrode. The inset of Fig. 9B illustrates the dependence of the electrocatalytic current on the concentration of NO_2^-. The response to NO_2^- is linear in the range from 5 μM to 22 mM (r^2 = 0.998). The detection limit was 5 μM at a S/N ratio of 3. When common anions such as 20 mM NO_3^-, 20 mM SO_4^-, 15 mM SO_3^-, and 15 mM CO_3^{2-} were tested with 200 μM NO_2^-, the catalytic current of NO_2^- was not depressed in the presence of these anions. On the basis of these results, NO_2^- can be selectively monitored using the Cu-NPs/PoPD/GCE.

The stability of the Cu-NPs/PoPD/GCE and the reproducibility of the electrochemical behavior were investigated by cyclic voltammetry. Under continuous potential sweeping at 100 mV s^{-1} between 0.2 and −0.9 V in 0.1 M PBS (pH 7.0), an insignificant decay in the peak currents was observed during the initial cycles (2% for the first 50 cycles), and the rate of current decrease then decreased (4% after 500 cycles), which indicated that the Cu-NPs/PoPD film is strongly attached to the electrode surface. The reproducibility of the Cu-NPs/PoPD/GCE was also investigated by measurement of the response to 100 μM H_2O_2 in 0.1 M PBS (pH 7.0). The RSD was 2.3% for seven successive additions. The RSD was 1.8% for the measurement of 100 μM NO_2^- in pH 1.0 aqueous solution (n = 7). The electrode fabrication reproducibility was examined at five different Cu-NPs/PoPD/GCEs prepared under the same conditions, and the RSD was 3.2%. On the basis of these results, the Cu-NPs/PoPD/GCE can be easily prepared and employed as an amperometric sensor for the determination of H_2O_2 and nitrite in real-sample analysis.

Conclusions

The electrochemical synthesis, characterization, and electrocatalytic properties of Cu-NPs incorporated into a PoPD film modified GCE and its application as an amperometric sensor for the detection of H_2O_2 and nitrite have been demonstrated. The Cu-NPs/PoPD/GCE shows excellent stability and electrocatalytic activity toward the reduction of H_2O_2 and nitrite. Cyclic voltammetry, EQCM, SEM, AFM, and XRD results reveal that Cu-NPs cover the electrode

surface. We have demonstrated a real-sample analysis of H_2O_2 using a Cu-NPs/PoPD/GCE, and the results obtained are satisfactory.

Acknowledgments

This work was financially supported by the Ministry of Education and the National Science Council of Taiwan.

National Taipei University of Technology assisted in meeting the publication costs of this article.

References

1. *Nanoparticles and Nanostructured Films*, J. H. Fendler, Editor, Wiley-VCH, Weinheim (1998).
2. *Catalysis and Electrocatalysis at Nanoparticle Surfaces*, A. Wieckowski, E. R. Savinova, and C. G. Vayenas, Editors, Marcel Dekker, New York (2003).
3. S. Trasatti, in *Electrochemistry of Novel Materials*, Chap. 5, J. Lipkowski and P. N. Ross, Editors, VCH, New York (1994).
4. *Nanotechnology in Catalysis*, Vols. 1 and 2, B. Zhou, S. Hermans, and G. A. Somerjai, Editors, Kluwer Academic/Plenum, London (2004).
5. C. M. Welch and R. G. Compton, *Anal. Bioanal. Chem.*, **384**, 601 (2006).
6. S. Hrapovic, Y. Liu, E. B. Male, and J. H. T. Luong, *Anal. Chem.*, **76**, 1083 (2004).
7. A. A. Karyakin, E. A. Puganova, I. A. Budashov, I. N. Kurochkin, E. E. Karyakin, V. A. Levchenko, V. N. Matveyenko, and S. D. Varfolomeyev, *Anal. Chem.*, **76**, 474 (2004).
8. L. D'Souza and S. Sampath, *Langmuir*, **16**, 8510 (2000).
9. R. Ramaraj, *J. Chem. Sci.*, **118**, 593 (2006).
10. E. Katz, I. Willner, and J. Wang, *Electroanalysis*, **16**, 19 (2004).
11. P. F. Fox and F. V. Kosikowski, *J. Dairy Sci.*, **45**, 648 (1962).
12. R. T. Toledo, *Food Technol.*, **29**, 5 (1975).
13. B. J. Juven and M. D. Pierson, *J. Food Prot*, **59**, 1233 (1996).
14. C.-L. Hsu, K.-S. Chang, and J.-C. Kuo, *Food Contr.*, **19**, 223 (2008).
15. J. Wang, M. Gu, J. Di, Y. Gao, Y. Wu, and Y. Tu, *Bioprocess Biosyst. Eng.*, **30**, 289 (2007).
16. G. Li, Y. Wang, and H. Xu, *Sensors*, **7**, 239 (2007).
17. X. Zhu, I. Yuri, X. Gan, I. Suzuki, and G. Li, *Biosens. Bioelectron.*, **22**, 1600 (2007).
18. S. A. Kumar and S. M. Chen, *Biosens. Bioelectron.*, **22**, 3042 (2007).
19. S. A. Kumar and S. M. Chen, *Talanta*, **72**, 831 (2007).
20. A. Salimi, A. Noorbakhsh, H. Mamkhezri, and R. Ghavami, *Electroanalysis*, **19**, 1100 (2007).
21. S. A. Kumar and S. M. Chen, *J. Mol. Catal. A: Chem.*, **278**, 244 (2007).
22. S. Yao, J. Xu, Y. Wang, X. Chen, Y. Xu, and S. Hu, *Anal. Chim. Acta*, **557**, 78 (2006).
23. K. S. Tseng, L. C. Chen, and K. C. Ho, *Sens. Actuators B*, **108**, 738 (2005).
24. S. A. Kumar, P.-H. Lo, and S.-M. Chen, *Nanotechnology*, **19**, 255501 (2008).
25. M. Barzegar, M. F. Mousavi, and A. Nemati, *Microchem. J.*, **65**, 159 (2000).
26. M. Thamae and T. Nyokong, *J. Electroanal. Chem.*, **470**, 126 (1999).
27. M. J. Moorcroft, J. Davis, and R. G. Compton, *Talanta*, **54**, 785 (2001).
28. A. T. Mubarak, A. A. Mohamed, K. F. Fawy, and A. S. Al-Shihry, *Microchim. Acta*, **157**, 99 (2007).
29. H. Chen, C. Mousty, L. Chen, and S. Cosnier, *Mater. Sci. Eng., C*, **28**, 726 (2008).
30. R. Geng, G. Zhao, M. Liu, and M. Li, *Biomaterials*, **29**, 2794 (2008).
31. S. T. Farrell and C. B. Breslin, *Electrochim. Acta*, **49**, 4497 (2004).
32. V. Tsakova and D. Borissov, *Electrochem. Commun.*, **2**, 511 (2000).
33. A. Zouaoui, O. Stephan, M. Carrier, and J. C. Moutet, *J. Electroanal. Chem.*, **474**, 113 (1999).
34. M. R. Guascito, P. Boffi, C. Malitesta, L. Sabbatini, and P. G. Zambonin, *Mater. Chem. Phys.*, **44**, 17 (1996).
35. I. Becerik and F. Kadirgan, *J. Electroanal. Chem.*, **436**, 189 (1997).
36. D. Schroer, R. J. Nichols, and H. Meyer, *Electrochim. Acta*, **40**, 1487 (1995).
37. Y. M. Zhu and C. R. Cabrera, *Electrochem. Solid-State Lett.*, **4**, A45 (2001).
38. M. J. Croissant, T. Napporn, J. M. Leger, and C. Lamy, *Electrochim. Acta*, **43**, 2447 (1998).
39. D. E. Stilwell and S. M. Park, *J. Electrochem. Soc.*, **135**, 2497 (1988).
40. D. K. Sarkar, X. J. Zhou, A. Tannous, and K. T. Leung, *J. Phys. Chem. B*, **107**, 2879 (2003).
41. K. Chiba, T. Ohsaka, Y. Ohnuki, and N. Oyama, *J. Electroanal. Chem.*, **219**, 117 (1987).
42. N. Oyama, T. Ohsaka, K. Chiba, and K. Takahashi, *Bull. Chem. Soc. Jpn.*, **61**, 1095 (1988).
43. J. Yano, *J. Polym. Sci., Part A: Polym. Chem.*, **33**, 2435 (1995).
44. H. P. Dai, Q. H. Wu, S. G. Sun, and K. K. Shiu, *J. Electroanal. Chem.*, **456**, 47 (1998).
45. K. Ogura, M. Kokura, J. Yano, and H. Shiigi, *Electrochim. Acta*, **40**, 2707 (1995).
46. S. R. Sivakkumar and R. Saraswathi, *J. Appl. Electrochem.*, **34**, 1147 (2004).
47. R. W. Murray, in *Electroanalytical Chemistry*, Vol. 13, A. J. Bard, Editor, pp. 191–368, Marcel Dekker, New York (1984).
48. G. Sauerbrey, *Z. Phys.*, **155**, 206 (1959).
49. V. Tsionsky, L. Daikhin, M. Urbakh, and E. Gileadi, in *Electroanalytical Chemistry*, Vol. 22, A. J. Bard and I. Rubinstein, Editors, pp. 1–99, Marcel Dekker, New York (2004).
50. M. Eyraud, S. Kologo, L. Bonou, and Y. Massiani, *J. Electroceram.*, **16**, 55 (2006).
51. M. E. Huerta Garrido and M. D. Pritzker, *J. Electrochem. Soc.*, **155**, D332 (2008).
52. B. Deng, A.-W. Xu, G.-Y. Chen, R.-Q. Song, and L. Chen, *J. Phys. Chem. B*, **110**, 11711 (2006).
53. M. Somasundrum, K. Kirtikara, and M. Tanticharoen, *Anal. Chim. Acta*, **319**, 59 (1996).
54. J. Zen, H. Chung, and A. S. Kumar, *Analyst (Cambridge, U.K.)*, **125**, 1633 (2000).
55. T. Wang, J.-S. Hu, W. Yang, and H.-M. Zhang, *Electrochem. Commun.*, **10**, 814 (2008).
56. P. Gajendran and R. Saraswathi, *J. Phys. Chem. C*, **111**, 11320 (2007).
57. F. A. Cotton and G. Wilkinson, *Advanced Inorganic Chemistry*, 4th ed., p. 430, John Wiley & Sons, New York (1980).
58. H. Wang, Y. Huang, Z. Tan, and X. Hu, *Anal. Chim. Acta*, **526**, 13 (2004).